Transition metal synthetic ferrimagnets: tuneable media for all optical switching driven by nanoscale spin current

Maciej Dąbrowski,[*,†] Jade N. Scott,[‡] William R. Hendren,[‡] Colin M. Forbes,[‡] Andreas Frisk,[¶] David M. Burn,[¶] David G. Newman,[†] Connor R. J. Sait,[†] Paul S. Keatley,[†] Alpha T. N'Diaye,[§] Thorsten Hesjedal,[‖] Gerrit van der Laan,[¶] Robert M. Bowman,[‡] and Robert J. Hicken[†]

†*Department of Physics and Astronomy, University of Exeter, Exeter, EX4 4QL, United Kingdom*

‡*School of Mathematics and Physics, Queen's University Belfast, Belfast, BT7 1NN, United Kingdom*

¶*Diamond Light Source, Harwell Science and Innovation Campus, Didcot, OX11 0DE, United Kingdom*

§*Advanced Light Source, Lawrence Berkeley National Laboratory, Berkeley, California 94720, USA*

‖*Department of Physics, Clarendon Laboratory, University of Oxford, OX1 3PU, United Kingdom*

E-mail: m.k.dabrowski@exeter.ac.uk

Abstract

All-optical switching of magnetization has great potential for use in future ultrafast and energy efficient nanoscale magnetic storage devices. So far, research was almost exclusively focused on rare-earth based materials, which limits device tunability and scalability. Here, we show that a perpendicularly magnetized synthetic ferrimagnet composed of two distinct transition metal ferromagnetic layers, Ni_3Pt and Co, can exhibit helicity independent magnetization switching. Switching occurs between two equivalent remanent states with antiparallel alignment of the Ni_3Pt and Co magnetic moments, and is observable over a broad temperature range. Time-resolved measurements indicate that the switching is driven by a spin-polarized current passing through the sub-nanometer Ir layer. The magnetic properties of this model system may be tuned continuously via sub-nanoscale changes in the constituent layer thicknesses as well as growth conditions, allowing the underlying mechanisms to be elucidated, and paving the way to a new class of data storage devices.

Keywords

all-optical magnetization switching, synthetic ferrimagnet, spintronics, magnetic recording, ultrafast spin current, negative remanence

Perpendicularly magnetized synthetic ferrimagnets (SFi) have attracted intense interest for stabilization of room-temperature skyrmions[1] and chiral exchange interaction,[2] fast domain wall motion,[3,4] spin-orbit torque switching[5] and all-optical switching (AOS) of magnetization.[6,7] Applications to magnetic recording are promising because the constituent layers of the SFi can be tailored independently to tune the AOS mechanism. So far, AOS has been observed principally within ferrimagnetic rare-earth transition metal (RE-TM) alloys[8–14] or SFis and spin valves containing RE atoms,[15–19] and only recently in the half-metallic compensated ferrimagnetic Heusler alloy Mn_2Ru_xGa,[20] and insulating ferrimagnet Co-substituted yttrium iron garnet.[21] In contrast, experimental studies of AOS in RE-free synthetic ferrimagnets[6,7] and ferromagnets[22] have been limited to helicity dependent AOS (HD-AOS). Theory predicts that helicity independent AOS (HI-AOS) can be achieved in antiferromagnetically coupled RE-free TM layers if the demagnetization rates of the two layers are substantially different,[23] but has not been experimentally observed.

Here, we demonstrate multi-pulse AOS in the SFi Ni_3Pt/Ir/Co, and show that the magnetic properties can be tuned through variation of the growth conditions and layer thicknesses, so that AOS can be achieved within a broad temperature range. Unlike previously studied systems exhibiting AOS, here the FM layers are magnetically soft, which leads to negative remanence for a range of temperatures below the compensation point T_M. Our results reveal that AOS occurs only for temperatures below the negative remanence regime, highlighting the importance of magnetic anisotropy, which has usually been assumed to play a lesser role.[24] In contrast to previous studies of RE-free SFis, we achieve HI-AOS. Time-resolved magneto-optical Kerr effect (TRMOKE) measurements indicate different demagnetization times of the Ni_3Pt and Co layers in the antiparallel (AP) state, and that a spin current generated during demagnetization is integral to the AOS process.

We prepared samples with thicknesses of 1 nm for the Co layer and 0.5 nm for the

Ir spacer, while the thickness and growth conditions of the Ni_3Pt were varied to tune the magnetic anisotropy and magnetization compensation temperature T_M at which the magnetic moments of the two layers cancel. Samples A, B, C, D and E, had T_M values of 271, 285, 310, 312 and 342 K, respectively. For all samples, the Curie temperature T_C of the Ni_3Pt layer, $310 - 350$ K, was much lower than for the Co, 780 K (Section S1 of the Supporting Information). Figure 1a shows the temperature dependence of the remanent magnetization for sample A. For the $|\mu_0 M_R|$ values shown by the blue line/squares, a 0.5 T saturating field, $\mu_0 H$, was applied at $T = 10$ K, $\mu_0 H$ was reduced to zero, and then the magnetization measured as the temperature was increased. Alternatively, $\mu_0 M_R$ was measured from hysteresis loops at every temperature point (red line/circles in Figure 1a). A compensation point is clearly evident at $T_M = 271$ K. Above (below) T_M the moment of the Co layer, m_{Co}, is larger (smaller) than that of Ni_3Pt, m_{Ni_3Pt}.

Above $T = 200$ K, $\mu_0 M_R$ begins to deviate towards negative values, reaching a negative extremum at around 240 K. SQUID hysteresis loops with positive and negative remanence are shown in Figure 1b and c, respectively. The appearance of negative remanence can be explained by considering the sum of the Zeeman energy, the interlayer exchange coupling (IEC) energy and the magnetic anisotropy (MA) energy.[25] Essentially, negative remanence can occur whenever the FM layer with the larger magnetic moment also has the smaller MA, so that it is energetically more favorable to switch the larger moment to achieve antiparallel alignment as $\mu_0 H$ is decreased,[25] increasing the Zeeman energy but minimising the MA and IEC energy. This is the case for most of the samples studied here since the MA of the Ni_3Pt falls off rapidly with increasing temperature, and becomes smaller than that of the Co at a temperature below T_M.[26]

Negative remanence has been observed in different multilayered thin films[25,27] and nanoparticles,[28] but remains unexplored in SFis. More insight into the magnetization reversal of $Ni_3Pt/Ir/Co$ is gained from element specific x-ray magnetic circular dichroism (XMCD) hysteresis loops. Below T_{-R}, Ni_3Pt exhibits a normal square hysteresis loop, while

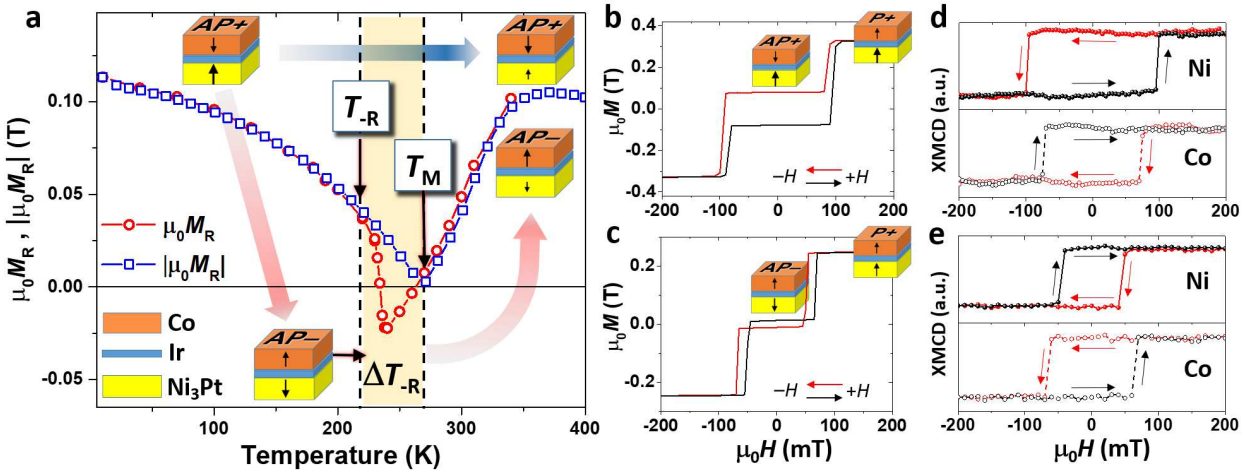

Figure 1: Magnetization reversal of $Ni_3Pt/Ir/Co$ (sample A). (a) Remanent magnetization as a function of temperature T obtained from SQUID, by measuring: i) the hysteresis loop at each temperature ($\mu_0 M_R$, red circles); ii) the remanent magnetization after reducing the applied field from saturation to zero at low temperature and then increasing T ($|\mu_0 M_R|$, blue squares). The blue and red arrows indicate how the trilayer moves between equivalent AP+ and AP− remanent states for the two measurement methods as T increases. Regions of the sample begin to exhibit negative remanence for temperatures above T_{-R}, so that the negative remanence region (beige shading) spans the temperature range $\Delta T_{-R} = T_M - T_{-R}$. (b,c) SQUID hysteresis loops acquired at (b) 150 K and (c) 250 K. (d,e) Element specific XMCD hysteresis loops acquired at the L_3 absorption edges of Ni and Co at (d) 150 K and (e) 250 K. Loops in (b,d) were acquired below T_{-R} (positive remanence), while (c,e) were acquired above T_{-R} but below T_M (negative remanence).

Co exhibits negative coercivity, i.e., for decreasing (increasing) field the magnetization becomes negative (positive) while $\mu_0 H$ is still positive (negative) (Figure 1d). Therefore, Co exhibits negative remanence while the total SFi remanent moment is positive because below T_M, $m_{Ni_3Pt} > m_{Co}$. Above T_{-R} the situation is opposite; Ni_3Pt exhibits negative coercivity while the Co exhibits a normal loop (Figure 1e). Below T_M this type of reversal can lead to negative remanence (Figure 1c). The transition to negative remanence appears gradual from SQUID magnetometry, due to formation of domains at remanence (Section S2, Supporting Information). The appearance of a negative remanence regime in Figure 1a indicates that the relative size of the magnetic anisotropies of the two layers can be tuned via the temperature. As we will show, this is an essential requirement for AOS between AP+ and AP− states.

We performed wide-field Kerr microscopy (WFKM) imaging of the SFi following pulsed laser excitation. The WFKM hysteresis loop in Figure 2a, obtained below T_{-R}, shows the magnetization reversal of both layers and the remanent states AP− and AP+ obtained after saturation at negative and positive fields. Depending upon the fluence F, pulse duration PD, and number of pulses N, optical pumping can result in formation of a domain structure (demagnetization) (Figure 2b) or AOS (Figure 2c-f). Uniform switching can only be achieved with reduced laser fluence, where the centre of the Gaussian beam induces a monodomain state.[29] For optimized pumping conditions, the remanent state can be switched back and forth, i.e., toggle switching is observed (Figure 2d). In contrast to HD-AOS in FM layers and previously studied RE-free SFis, here switching is polarization/helicity independent. The larger switched regions in Figure 2c exhibit less reproducible toggling. Where toggle switching was observed, the switched regions do not exceed 10 μm diameter (Figure 2d and 2e). We could not achieve AOS with a single pulse ($N = 1$), and regardless of N, the pump helicity does not affect the final state. Optical pumping with $\mu_0 H$ applied normal to the sample plane demonstrates that switching can be either promoted or hindered by $\mu_0 H$ oriented antiparallel or parallel to

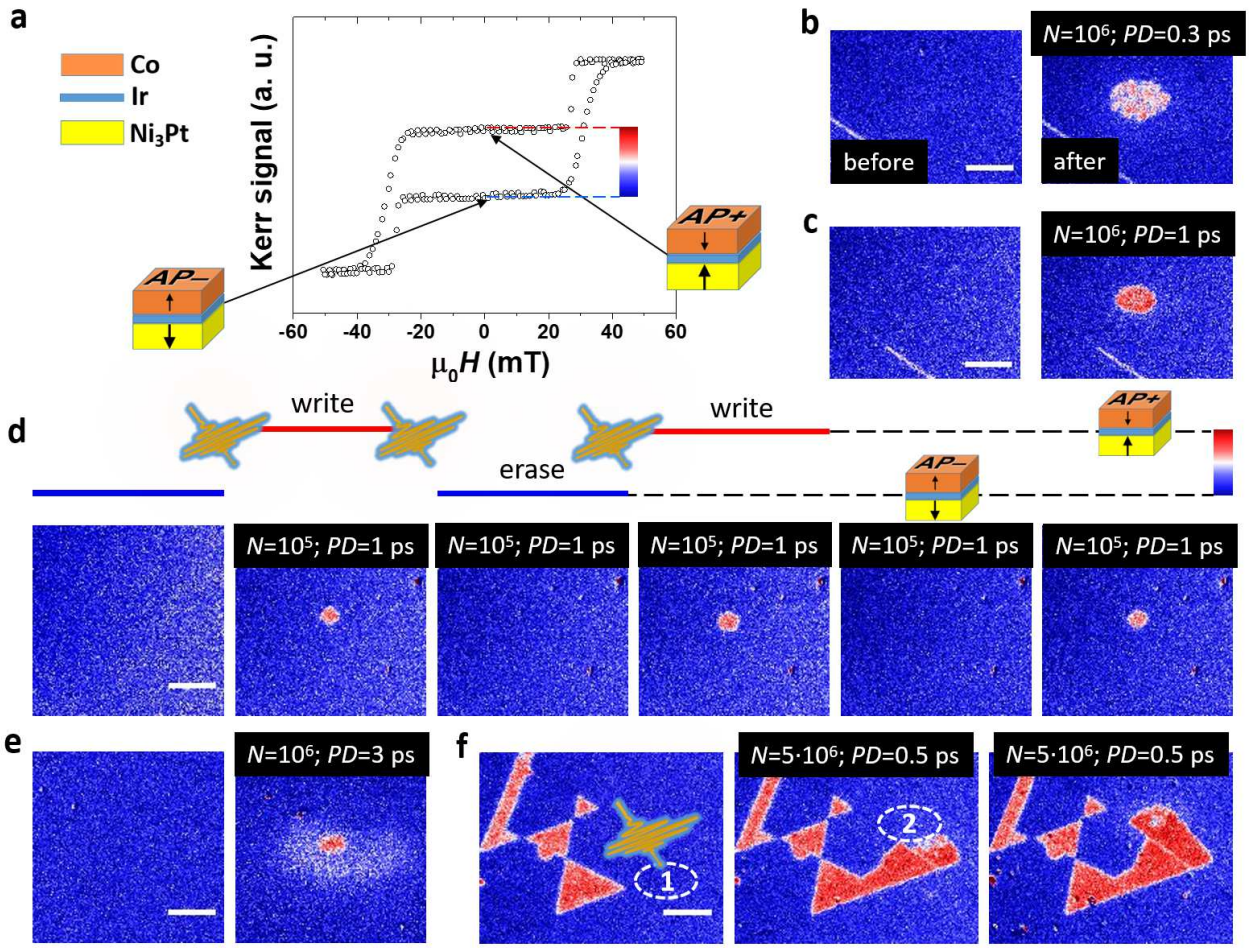

Figure 2: Observation of all-optical switching. (a) MOKE hysteresis loop and corresponding magnetization configurations for the SFi at remanence, for temperatures below $T_{\text{-R}}$. (b) Demagnetization/domain formation, (c) AOS and (d) toggle switching, induced with fluence $F = 10\,\text{mJ/cm}^2$ at 230 K for sample B. Schematic in (d) illustrates how the toggle switching between the AP+ and AP− remanent states allows to write and erase magnetic bits with consecutive pulses. (e) Toggle switching with $F = 13\,\text{mJ/cm}^2$ at 280 K for sample C. (f) AOS with $F = 10\,\text{mJ/cm}^2$ for sample E. The region to be excited is shown by the white dashed ellipse while the resulting magnetic state is shown in the next frame. Both pumped areas labeled '1' and '2' exhibit AOS, as shown in the second and third frames, respectively. In all cases σ^- polarization and a pump spot size diameter of 90 μm (intensity at $1/e^2$) were used, while the number of pulses N and the pulse duration PD is shown for each measurement. The scale bar has length of 20 μm.

the magnetization of the Co, respectively. Hence, the final ordering of the ferrimagnet is dictated by the Co layer (FM with higher T_C). For long exposure times, such as for $N = 5 \cdot 10^6$ in Figure 2f, we can achieve uniform switching, but the shape and size of the switched regions is determined by the exact surface topography and variations in local magnetic parameters. More information about the demagnetization and AOS is presented in Sections S3 and S4 of the Supporting Information .

The results obtained with fixed pump spot position show that, even though full AOS is possible, the spot's Gaussian intensity profile hinders uniform switching of areas larger than $\sim 20\,\mu$m. Such behaviour is common to most materials exhibiting multi-pulse AOS and, in general, it is easier to achieve uniform switching by sweeping the beam.[22,30,31] We recorded Kerr images after sweeping the beam across the sample surface. Figure 3 shows the occurrence of AOS for sample D as a function of temperature T and fluence F. Uniform HI-AOS is seen for a wide range of fluence, but only for $T < T_{\text{-R}}$. The widest temperature range for AOS observed in a single sample is from 90 - 270 K (Section S5, Supporting Information).

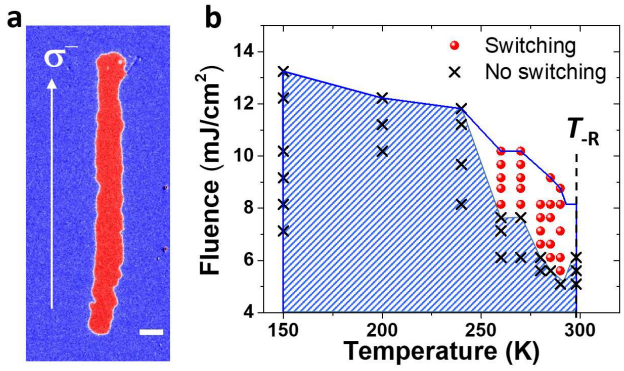

Figure 3: (a) Image of switching induced by a swept beam for sample D. (b) Diagram showing the switching behavior as a function of sample temperature T and fluence F for sample D. In all cases σ^- polarization, a pump spot size diameter of $90\,\mu$m (intensity at $1/e^2$), pulse duration of 1 ps, and 1 MHz repetition rate were used. The scale bar has length of $20\,\mu$m.

As we demonstrated in Figure 2, toggle switching is helicity independent and cannot be explained by either the magnetic circular dichroism (MCD) effect[30] or the inverse

Faraday effect (IFE).[32] The question arises whether transfer of spin angular momentum between layers[33] plays a role in AOS in the present case? It is known that ultrafast demagnetization can generate a transient spin current, with the flux of spin angular momentum proportional to $-dM/dt$.[18,33–35] We therefore performed TRMOKE experiments in which a probe pulse is delayed by time τ_d relative to the pump pulse (Figure 4a). Figure 4b shows ultrafast demagnetization (ps time scales) and remagnetization (ns time scales) for the saturated and remanent states, which correspond to parallel P+ and antiparallel AP+ alignment of the layer magnetizations, respectively, as shown in Figure 4a. For the P+ state, nearly full demagnetization of both layers is achieved after 790 fs for $F = 6.9\,\mathrm{mJ/cm^2}$, with no indication of different demagnetization time τ_M for the two layers, consistent with measurements performed on separate Ni_3Pt and Co reference samples (Section S6, Supporting Information). In contrast, for the AP+ state, the Kerr signal exhibits a minimum at τ_d = 350 fs, and a local maximum at τ_d = 790 fs. Coincidentally, the Kerr rotations originating from the two layers are of the same magnitude but opposite sign for this sample (see Fig. 4a), allowing us to qualitatively identify differences in demagnetization times. Because we know the initial orientation of the layer magnetizations (Figure 4a), we deduce that the peak at 350 fs corresponds to full demagnetization of Ni_3Pt while the subsequent increase until about 790 fs is due to demagnetization of the Co layer. Hence, we observe faster demagnetization of Ni_3Pt in the AP state in comparison to the P state, which indicates a transfer of spin angular momentum between the layers.[33] This assumes no gain of magnetization due to spin current before the Ni_3Pt has fully demagnetized since this is not expected for the AP state.[36] The subsequent gradual increase of the signal, for $\tau_d > 1$ ps to τ_d = 500 ps, is associated with the different remagnetization rates of Ni_3Pt and Co, and is reproduced by plotting the difference of the signals acquired from separate Ni_3Pt and Co reference samples (Section S6, Supporting Information).

To further explore the effect of the different τ_M values of Ni_3Pt and Co, we plot the TRMOKE signal for the AP+ state for different F in Figure 4c. For the smallest

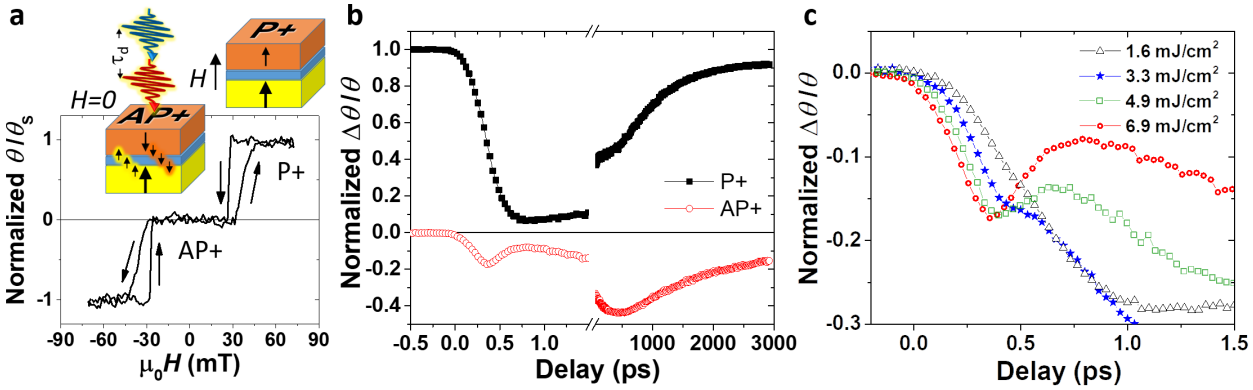

Figure 4: Ultrafast demagnetization and transfer of spin angular momentum. (a) Schematic of the experimental geometry for TRMOKE experiments and Kerr hysteresis loop obtained with a 400 nm laser probe. (b) TRMOKE signal $\Delta\theta/\theta$ in the saturation (P+) and remanent (AP+) state for fluence $F = 6.9\,\mathrm{mJ/cm^2}$. (c) Fluence dependence of the ultrafast demagnetization in the AP+ state. The size of the TRMOKE signal $\Delta\theta/\theta$ is normalized to the height of the static Kerr hysteresis loop θ/θ_S measured with the same laser probe as shown in (a), so that the size of the optically induced magnetization change can be estimated. The measurements were performed at room temperature for sample E.

fluence, no minimum is observed at $\tau_d \approx 350\,\mathrm{fs}$ since the Co experiences only small demagnetization and the Ni_3Pt demagnetizes on a timescale comparable to the reference films. As F is increased to $3.3\,\mathrm{mJ/cm^2}$ an inflection point appears. Further increasing F, as the inflection becomes a minimum, the signal magnitude at this point remains nearly constant, but the minimum shifts towards smaller time delay. This confirms that the initial peak originates from Ni_3Pt, which is expected to fully demagnetize for all the displayed fluence values. Most importantly, τ_M decreases with increasing F, confirming the presence of spin angular momentum transfer between layers in the AP state,[33] because otherwise increasing F would cause τ_M to increase.[37] We do not attempt to identify the nature of the spin angular momentum transfer, but can assume that either 'superdiffusive spin current',[36,38] 'diffusive spin current'[34,35] or transduction of magnon spin current[24] at the Ir interfaces could contribute to the magnetization switching. One possible scenario is that, as for [Co/Pt]/Cu/GdFeCo,[17] the layer with longer τ_M (Co) sets the direction of the magnetization in the other layer (Ni_3Pt). During remagnetization, the Co reorients to maintain the AP state. Since AOS is only observed for $T < T_{-R}$, the final reorientation

of the Co layer depends upon the anisotropy field of the Ni_3Pt being larger than that of the Co during the reorientation process. All samples studied here appear to possess essentially the same AOS properties, even though we were not able to acquire complete sets of data with all of the different techniques for all of the samples. The only significant difference between the AOS observed in different samples is the temperature range through which the AOS can be observed at a given fluence. As we have demonstrated, it is not the compensation point T_M but the transition to the negative remanence T_{-R} that limits the range of temperature in which AOS can be observed, highlighting the importance of the magnetic anisotropy for the AOS in SFi with RE-free TM layers.

In summary, our results demonstrate that magnetization switching in a SFi composed of RE-free TM layers can be achieved using femtosecond laser pulses and without an applied magnetic field. In contrast to the single pulse HI-AOS observed in RE-TM alloys[8–12] and Mn_2Ru_xGa alloys,[20] here we can only observe multi-pulse HI-AOS. The main reason for the different AOS properties is that in the SFi studied here, there are two separate ferromagnetic layers coupled through an interlayer exchange coupling (IEC) that is much weaker than the direct exchange coupling found in ferrimagnetic alloys. To the best of our knowledge, the IEC of $Ni_3Pt/Ir/Co$ ($J_{IEC} = -1.8x10^{-22}$ J/link[26]) is the lowest among materials exhibiting AOS, and two orders of magnitude smaller than the theoretical threshold for single pulse switching of a SFi.[23] Although larger magnetic anisotropy for one of the layers and stronger interlayer coupling might be required for single pulse AOS,[23,24] we have taken advantage of the smaller saturation field to explore the ground state and its broad tunability. However, as for the case of RE-TM and Mn_2Ru_xGa alloys, a transfer of angular momentum between the sublattices/layers, which leads to a transient ferromagnetic-like state,[9] appears to be a key ingredient for the HI-AOS of the SFi presented here. SFis with two distinct TM layers are highly suited to experiments with element-specific probes,[9] while the local nature of the reversal mechanism is amenable to atomistic calculations.[23] Finally, the SFis presented here are

based upon elemental transition metals, which allows for a simplified and low cost fabrication process, and scaling down of AOS device sizes. $Ni_3Pt/Ir/Co$ is therefore a model system that provides new understanding of the process of AOS, as well as a promising medium for future photo-magnetic recording.

METHODS

Sample fabrication. Samples were fabricated via RF and DC sputtering from elemental targets, with base pressure 10^{-9} Torr and sputtering pressure of 10^{-3} Torr with Ar^{+}. Three different substrates were used: *c*-plane Al_2O_3, *r*-plane Al_2O_3 and Si/SiO_2, with a Ta(5) seed layer in each case. Perpendicular anisotropy in Ni_3Pt alloys requires deposition at elevated temperatures,[26] and in thin Co films through interfacing with Ir. SFi samples were produced using a 2-stage process, firstly depositing Ta/Ni_3Pt at elevated temperature, before cooling under vacuum overnight for the second stage, RT deposition of Ir(0.5nm)/Co(1nm)/Ir(3nm). The following samples were presented in this work (sample name: substrate, deposition temperature of Ni_3Pt, Ni_3Pt thickness in nm, compensation point T_M):

Sample A: *r*-plane Al_2O_3, 536 K, Ni_3Pt(8.5), 271 K;

Sample B: *c*-plane Al_2O_3, 540 K, Ni_3Pt(8.5), 285 K ;

Sample C: Si/SiO_2, 473 K, Ni_3Pt(10), 310 K;

Sample D: *c*-plane Al_2O_3, 576 K, Ni_3Pt(10), 312 K;

Sample E: *c*-plane Al_2O_3, 544 K, Ni_3Pt(11), 342 K.

Note that fabrication of the SFi structures does not depend upon lattice engineering of the substrate, and the choice of Al_2O_3 substrates for many of the samples was to enable XMCD measurements in which x-ray excited optical luminescence in the Al_2O_3 substrate provides the measured signal.

X-ray magnetic circular dichroism (XMCD). Element-specific XMCD hysteresis loops and spectra were measured at beamlines I10 of the Diamond Light Source (DLS) and 6.3.1 of the Advanced Light Source (ALS) to probe the reversal of the Ni_3Pt and Co independently. The x-ray wavevector was parallel to the applied magnetic field, normal to the sample plane.

Wide-field Kerr microscopy (WFKM). The polar Kerr effect was used to sense the out-of-

plane magnetization in response to either a magnetic field or optical pulses. The sample illumination was linearly polarized, while polarization changes of the reflected light due to the polar Kerr effect were detected as intensity changes using a nearly crossed analyzer, quarter-waveplate, and high sensitivity CMOS camera. In some cases, differential imaging was used to subtract non-magnetic contrast such as sample topography. For AOS experiments, an optical pump beam of variable polarization, pulse duration and repetition rate was incident at 45° to the sample plane and focused to a 90 μm diameter spot (intensity at $1/e^2$). In most experiments the fundamental output of the laser at 1035 nm was used. In a few experiments, an optical parametric amplifier (OPA) with output tunable from 650 nm to 900 nm and with fixed pulse duration of 25 fs was employed. Measurements were performed from ambient temperatures in the range 80 - 310 K.

Time-resolved magneto-optical Kerr effect (TRMOKE). Optically induced magnetization dynamics were probed using an amplified Ti:sapphire pulsed laser source with either 20 kHz or 100 kHz repetition rate and 35 fs pulse width. The s-polarized 800 nm pump and p-polarized 400 nm probe beams were incident normal, and at 10° from the surface normal, respectively, and focused to 100 μm and 30 μm diameter spots (at $1/e^2$). All TRMOKE measurements were performed at room temperature.

Supporting Information Available

The Supporting Information is available free of charge.

- S1. Sample characterization. S2. XMCD hysteresis loops and domain structure. S3. Optically induced domain structure creation and bias field assisted switching. S4. Additional AOS results. S5. AOS with the beam swept along the sample surface. S6. TRMOKE and transfer of spin angular momentum.

Acknowledgement

We thank R. F. L. Evans for critical reading of the manuscript. The authors acknowledge the Engineering and Physical Sciences Research Council (EPSRC) under Grant Numbers EP/P021190/1, EP/P020151/1, and EP/P02047X/1. The Exeter Time-Resolved Magnetism Facility (EXTREMAG - EPSRC Grant Reference EP/R008809/1) is acknowledged. Beamtime awarded on I10 at the Diamond Light Source (SI17745-1, SI19116-1 and SI20760-1) is acknowledged. This research used resources of the Advanced Light Source, which is a DOE Office of Science User Facility under contract no. DE-AC02-05CH11231. J.S. acknowledges prior support via the EPSRC Centre for Doctoral Training in Photonic Integration & Advanced Data Storage (Grant No. EP/L015323/01). The contributions of R.M.B. & J.S. to the project were supported by the Royal Academy of Engineering under the Research Chairs and Senior Research Fellowships Scheme. R.M.B. & W.H. acknowledge the support of Seagate Technology (Ireland) under SOW #00077300.0. D.G.N. and C.R.J.S. acknowledge support via the EPSRC Centre for Doctoral Training in Metamaterials (Grant No. EP/L015331/1).

Author Contributions

M.D., R.M.B. and R.J.H. coordinated the project; M.D. performed Kerr imaging and TRMOKE measurements; J.N.S., W.R.H., C.M.F. and R.M.B. grew, characterized and optimized the samples; J.N.S. and W.R.H. performed SQUID measurements; M.D., A.F., D.M.B., D.G.N. and A.T.N. performed XMCD measurements; M.D. and P.S.K. set up AOS experiment; M.D. and R.J.H. wrote the paper, with contributions from all authors.

Notes

The authors declare no competing financial interest.

References

(1) Legrand, W.; Maccariello, D.; Ajejas, F.; Collin, S.; Vecchiola, A.; Bouzehouane, K.; Reyren, N.; Cros, V.; Fert, A. Room-temperature stabilization of antiferromagnetic skyrmions in synthetic antiferromagnets. *Nat. Mater.* **2020**, *19*, 34–42.

(2) Han, D.-S.; Lee, K.; Hanke, J.-P.; Mokrousov, Y.; Kim, K.-W.; Yoo, W.; van Hees, Y. L. W.; Kim, T.-W.; Lavrijsen, R.; You, C.-Y.; Swagten, H. J. M.; Jung, M.-H.; Kläui, M. Long-range chiral exchange interaction in synthetic antiferromagnets. *Nat. Mater.* **2019**, *18*, 703–708.

(3) Yang, S.-H.; Ryu, K.-S.; Parkin, S. Domain-wall velocities of up to 750 m s^{-1} driven by exchange−coupling torque in synthetic antiferromagnets. *Nat. Nanotechnol.* **2015**, *10*, 221–226.

(4) Kim, K.-J.; Kim, S. K.; Hirata, Y.; Oh, S.-H.; Tono, T.; Kim, D.-H.; Okuno, T.; Ham, W. S.; Kim, S.; Go, G.; Tserkovnyak, Y.; Tsukamoto, A.; Moriyama, T.; Lee, K.-J.; Ono, T. Fast domain wall motion in the vicinity of the angular momentum compensation temperature of ferrimagnets. *Nat. Mater.* **2017**, *16*, 1187–1192.

(5) Zhang, P. X.; Liao, L. Y.; Shi, G. Y.; Zhang, R. Q.; Wu, H. Q.; Wang, Y. Y.; Pan, F.; Song, C. Spin-orbit torque in a completely compensated synthetic antiferromagnet. *Phys. Rev. B* **2018**, *97*, 214403.

(6) Mangin, S.; Gottwald, M.; Lambert, C.-H.; Steil, D.; Uhlíř, V.; Pang, L.; Hehn, M.; Alebrand, S.; Cinchetti, M.; Malinowski, G.; Fainman, Y.; Aeschlimann, M.; Fullerton, E. E. Engineered materials for all-optical helicity-dependent magnetic switching. *Nat. Mater.* **2014**, *13*, 286–292.

(7) Liao, J.-W.; Vallobra, P.; O'Brien, L.; Atxitia, U.; Raposo, V.; Petit, D.; Vemulkar, T.; Malinowski, G.; Hehn, M.; Martínez, E.; Mangin, S.; Cowburn, R. P. Controlling

All-Optical Helicity-Dependent Switching in Engineered Rare-Earth Free Synthetic Ferrimagnets. *Adv. Sci.* **2019**, *9*, 1901876.

(8) Stanciu, C. D.; Hansteen, F.; Kimel, A. V.; Kirilyuk, A.; Tsukamoto, A.; Itoh, A.; Rasing, T. All-Optical Magnetic Recording with Circularly Polarized Light. *Phys. Rev. Lett.* **2007**, *99*, 047601.

(9) Radu, I.; Vahaplar, K.; Stamm, C.; Kachel, T.; Pontius, N.; Dürr, H. A.; Ostler, T. A.; Barker, J.; Evans, R. F. L.; Chantrell, R. W.; Tsukamoto, A.; Itoh, A.; Kirilyuk, A.; Rasing, T.; Kimel, A. V. Transient ferromagnetic-like state mediating ultrafast reversal of antiferromagnetically coupled spins. *Nature* **2011**, *472*, 205–208.

(10) Ostler, T. A. et al. Ultrafast heating as a sufficient stimulus for magnetization reversal in a ferrimagnet. *Nat. Commun.* **2012**, *3*, 666.

(11) Hassdenteufel, A.; Hebler, B.; Schubert, C.; Liebig, A.; Teich, M.; Helm, M.; Aeschlimann, M.; Albrecht, M.; Bratschitsch, R. Thermally Assisted All-Optical Helicity Dependent Magnetic Switching in Amorphous $Fe_{100-x}Tb_x$ Alloy Films. *Adv. Mater.* **2013**, *25*, 3122–3128.

(12) Graves, C. E. et al. Nanoscale spin reversal by non-local angular momentum transfer following ultrafast laser excitation in ferrimagnetic GdFeCo. *Nat. Mater.* **2013**, *12*, 293–298.

(13) Xu, Y.; Deb, M.; Malinowski, G.; Hehn, M.; Zhao, W.; Mangin, S. Ultrafast Magnetization Manipulation Using Single Femtosecond Light and Hot-Electron Pulses. *Adv. Mater.* **2017**, *29*, 1703474.

(14) Iacocca, E. et al. Spin-current-mediated rapid magnon localisation and coalescence after ultrafast optical pumping of ferrimagnetic alloys. *Nat. Commun.* **2019**, *10*, 1756.

(15) Lalieu, M. L. M.; Peeters, M. J. G.; Haenen, S. R. R.; Lavrijsen, R.; Koopmans, B. Deterministic all-optical switching of synthetic ferrimagnets using single femtosecond laser pulses. *Phys. Rev. B* **2017**, *96*, 220411(R).

(16) Gorchon, J.; Lambert, C.-H.; Yang, Y.; Pattabi, A.; Wilson, R. B.; Salahuddin, S.; Bokor, J. Single shot ultrafast all optical magnetization switching of ferromagnetic Co/Pt multilayers. *Appl. Phys. Lett.* **2017**, *111*, 042401.

(17) Iihama, S.; Xu, Y.; Deb, M.; Malinowski, G.; Hehn, M.; Gorchon, J.; Fullerton, E. E.; Mangin, S. Single-Shot Multi-Level All-Optical Magnetization Switching Mediated by Spin Transport. *Adv. Mater.* **2018**, *30*, 1804004.

(18) Igarashi, J.; Remy, Q.; Iihama, S.; Malinowski, G.; Hehn, M.; Gorchon, J.; Hohlfeld, J.; Fukami, S.; Ohno, H.; Mangin, S. Engineering Single-Shot All-Optical Switching of Ferromagnetic Materials. *Nano Lett.* **2020**, *20*, 8654–8660

(19) van Hees, Y. L. W.; van de Meugheuvel, P.; Koopmans, B.; Lavrijsen, R. Deterministic all-optical magnetization writing facilitated by non-local transfer of spin angular momentum. *Nat. Commun.* **2020**, *11*, 3835.

(20) Banerjee, C.; Teichert, N.; Siewierska, K. E.; Gercsi, Z.; Atcheson, G. Y. P.; Stamenov, P.; Rode, K.; Coey, J. M. D.; Besbas, J. Single pulse all-optical toggle switching of magnetization without gadolinium in the ferrimagnet Mn_2Ru_xGa. *Nat. Commun.* **2020**, *11*, 4444.

(21) Stupakiewicz, A.; Szerenos, K.; Afanasiev, D.; Kirilyuk, A.; Kimel, A. V. Ultrafast nonthermal photo-magnetic recording in a transparent medium. *Nature* **2017**, *542*, 71–74.

(22) Lambert, C.-H.; Mangin, S.; Varaprasad, B. S. D. C. S.; Takahashi, Y. K.; Hehn, M.; Cinchetti, M.; Malinowski, G.; Hono, K.; Fainman, Y.; Aeschlimann, M.; Fuller-

ton, E. E. All-optical control of ferromagnetic thin films and nanostructures. *Science* **2014**, *345*, 1337–1340.

(23) Evans, R. F. L.; Ostler, T. A.; Chantrell, R. W.; Radu, I.; Rasing, T. Ultrafast thermally induced magnetic switching in synthetic ferrimagnets. *Appl. Phys. Lett.* **2014**, *104*, 082410.

(24) Barker, J.; Atxitia, U.; Ostler, T. A.; Hovorka, O.; Chubykalo-Fesenko, O.; Chantrell, R. W. Two-magnon bound state causes ultrafast thermally induced magnetisation switching. *Sci. Rep.* **2013**, *3*, 3262.

(25) Takanashi, K.; Kurokawa, H.; Fujimori, H. A novel hysteresis loop and indirect exchange coupling in Co/Pt/Gd/Pt multilayer films. *Appl. Phys. Lett.* **1993**, *63*, 1585–1587.

(26) Scott, J. A Combined Experimental and Computational Study of Ni3Pt/Ir/Co Synthetic Ferrimagnets: Taking Atomistic Spin Simulation into the Laboratory. *PhD thesis (Queen's University Belfast)* **2020**,

(27) Kim, D.; Kim, C.; Kim, C.-O.; Yoon, S. S.; Naka, M.; Tsunoda, M.; Takahashi, M. Negative coercivity characteristics in antiferromagnetic coupled hard/soft multilayers. *J. Magn. Magn. Mater.* **2006**, *304*, e356–e358.

(28) Yan, X.; Xu, Y. Negative remanence in magnetic nanostructures. *J. Appl. Phys.* **1996**, *79*, 6013–6015.

(29) Vomir, M.; Albrecht, M.; Bigot, J.-Y. Single shot all optical switching of intrinsic micron size magnetic domains of a Pt/Co/Pt ferromagnetic stack. *Appl. Phys. Lett.* **2017**, *111*, 242404.

(30) Khorsand, A. R.; Savoini, M.; Kirilyuk, A.; Kimel, A. V.; Tsukamoto, A.; Itoh, A.;

Rasing, T. Role of Magnetic Circular Dichroism in All-Optical Magnetic Recording. *Phys. Rev. Lett.* **2012**, *108*, 127205.

(31) Parlak, U.; Adam, R.; Bürgler, D. E.; Gang, S.; Schneider, C. M. Optically induced magnetization reversal in $[Co/Pt]_N$ multilayers: Role of domain wall dynamics. *Phys. Rev. B* **2018**, *98*, 214443.

(32) Kimel, A. V.; Kirilyuk, A.; Usachev, P. A.; Pisarev, R. V.; Balbashov, A. M.; Rasing, T. Ultrafast non-thermal control of magnetization by instantaneous photomagnetic pulses. *Nature* **2005**, *435*, 655–657.

(33) Malinowski, G.; Dalla Longa, F.; Rietjens, J. H. H.; Paluskar, P. V.; Huijink, R.; Swagten, H. J. M.; Koopmans, B. Control of speed and efficiency of ultrafast demagnetization by direct transfer of spin angular momentum. *Nat. Phys.* **2008**, *4*, 855–858.

(34) Choi, G.-M.; Min, B.-C.; Lee, K.-J.; Cahill, D. G. Spin current generated by thermally driven ultrafast demagnetization. *Nat. Commun.* **2014**, *5*, 4334.

(35) Choi, G.-M.; Min, B.-C. Laser-driven spin generation in the conduction bands of ferrimagnetic metals. *Phys. Rev. B* **2018**, *97*, 014410.

(36) Rudolf, D. et al. Ultrafast magnetization enhancement in metallic multilayers driven by superdiffusive spin current. *Nat. Commun.* **2012**, *3*, 1037.

(37) Koopmans, B.; Malinowski, G.; Dalla Longa, F.; Steiauf, D.; Fahnle, M.; Roth, T.; Cinchetti, M.; Aeschlimann, M. Explaining the paradoxical diversity of ultrafast laser-induced demagnetization. *Nat. Mater.* **2010**, *9*, 259–265.

(38) Battiato, M.; Carva, K.; Oppeneer, P. M. Superdiffusive Spin Transport as a Mechanism of Ultrafast Demagnetization. *Phys. Rev. Lett.* **2010**, *105*, 027203.

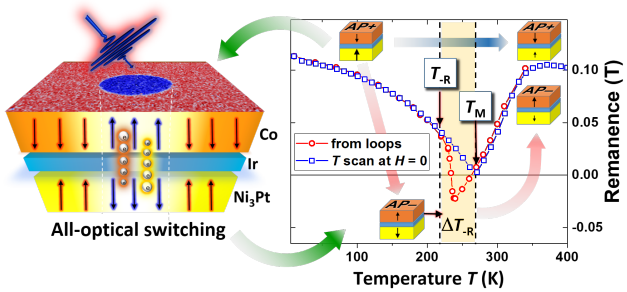

For Table of Contents Only